# Release of Native-like Gaseous Proteins from Electrospray Droplets via the Charged Residue Mechanism: Insights from Molecular Dynamics Simulations

Robert G. McAllister, Haidy Metwally, Yu Sun, and Lars Konermann*

Department of Chemistry, The University of Western Ontario, London, Ontario N6A 5B7, Canada

Ⓢ *Supporting Information*

ABSTRACT: The mechanism whereby gaseous protein ions are released from charged solvent droplets during electrospray ionization (ESI) remains a matter of debate. Also, it is unclear to what extent electrosprayed proteins retain their solution structure. Molecular dynamics (MD) simulations offer insights into the temporal evolution of protein systems. Surprisingly, there have been no all-atom simulations of the protein ESI process to date. The current work closes this gap by investigating the behavior of protein-containing aqueous nanodroplets that carry excess positive charge. We focus on "native ESI", where proteins initially adopt their biologically active solution structures. ESI proceeds while the protein remains entrapped within the droplet. Protein release into the gas phase occurs upon solvent evaporation to dryness. Droplet shrinkage is accompanied by ejection of charge carriers (Na$^+$ for the conditions chosen here), keeping the droplet at ~85% of the Rayleigh limit throughout its life cycle. Any remaining charge carriers bind to the protein as the final solvent molecules evaporate. The outcome of these events is largely independent of the initial protein charge and the mode of charge carrier binding. ESI charge states and collision cross sections of the MD structures agree with experimental data. Our results confirm the Rayleigh/charged residue model (CRM). Field emission of excess Na$^+$ plays an ancillary role by governing the net charge of the shrinking droplet. Models that envision protein ejection from the droplet are not supported. Most nascent CRM ions retain native-like conformations. For unfolded proteins ESI likely proceeds along routes that are different from the native state mechanism explored here.
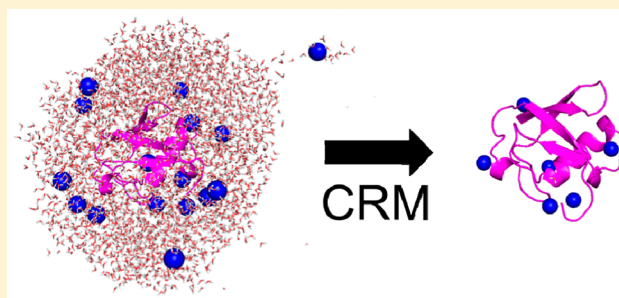
INTRODUCTION

Electrospray ionization (ESI) allows the production of desolvated ions from proteins and protein complexes in solution.[1] Analysis of these gaseous biomolecular systems by mass spectrometry (MS) reveals the nature of protein interaction partners while simultaneously reporting on binding stoichiometries.[2−4] Ion mobility spectrometry (IMS),[5−8] dissociation experiments,[9−12] and soft landing studies[13] provide additional insights. The gas phase represents an unusual environment for biomolecules.[14] Yet, under properly optimized conditions many[13,15−17] (but not all[9,18]) proteins seem to survive the ESI process in solution-like conformations that are kinetically stable on a μs−ms time scale. For these so-called "native" ESI-MS studies[2−4] proteins are electrosprayed in neutral aqueous solution with minimum activation along the ion path. Gaseous proteins formed by native ESI exhibit relatively low charge states.[19] This aspect favors the retention of compact structures by minimizing internal Coulomb repulsion.[8]

The ESI process starts with droplets of analyte solution that are emitted from a Taylor cone into a heated gas environment. These droplets are positively charged due to the presence of excess H$^+$, NH$_4^+$ or Na$^+$.[20] The production of negative droplets is possible as well, but here we focus on the commonly used positive ion mode. Solvent evaporation increases the charge density until jet fission gives rise to the formation of smaller offspring droplets.[21,22] These fission events take place slightly below the Rayleigh limit,[21−23] which is defined by[20]

$$z_R = \frac{8\pi}{e}\sqrt{\varepsilon_0 \gamma r^3} \tag{1}$$

where z_R is the number of net charges, r is the droplet radius, ε_0 is the vacuum permittivity, γ is the surface tension (0.05891 N m^{-1} for water at 370 K),[24] and $e = 1.602 \times 10^{-19}$ C. Repeated evaporation/fission events ultimately produce charged nanodroplets from which analyte ions are released into the gas phase.[20] Residual solvent molecules are removed by collisional activation as the ions travel through a sampling interface into the vacuum of the mass spectrometer.[25]

The early stages of droplet evolution have been extensively studied by electrodynamic balance measurements,[23] phase Doppler anemometry,[22] and imaging experiments.[21,26,27] Unfortunately, these techniques are not applicable to late ESI nanodroplets due to the small size and short lifetimes of these systems.[20] Thus, uncertainties persist regarding the final steps by which gaseous analyte ions are produced. According to the

ion evaporation model (IEM) the electrostatic field at the nanodroplet surface triggers analyte ejection.[28,29] Conversely, the charged residue model (CRM) envisions that gaseous analytes are released when nanodroplets evaporate to dryness.[30] It is often claimed that the IEM applies to low molecular weight species, whereas the CRM is operative for large globular analytes such as natively folded proteins.[20] A third scenario, the chain ejection mechanism (CEM), may account for the behavior of disordered polymers. In the CEM the analyte chain gets extruded from the droplet surface.[4,31,32] The fact that unfolded proteins form much higher charge states than compact conformers has been attributed to proton equilibration between the droplet and the protruding chain.[32]

The CRM is considered by many to be the most likely scenario for native protein ESI.[20,32,33] Support for this view comes from the observation that the charge states z of $[M + zH]^{z+}$ ions in native ESI are close to the z_R value of protein-sized water droplets eq 1.[20,34] Also, the tendency of native proteins to form nonspecific adducts is consistent with the idea that residual nonvolatile species will cluster together as the final solvent layers vanish.[35] Nonetheless, the CRM is not universally accepted.[36,37] Some researchers favor combined CRM/IEM models.[38,39] Others believe that the IEM applies to both small and large analytes, all the way to proteins.[40] While it is relatively straightforward to envision how the Rayleigh charge/CRM framework can govern the ESI charge states of proteins that are initially neutral, it is not so obvious what would happen for proteins that carry an initial nonzero charge.[41] It has also been noted[42] that charge states are not always consistent with the γ-dependence implied by eq 1.[34] Attempts have been made to understand charge states in native ESI on the basis of apparent gas phase basicities,[37,43] instead of relying on the Rayleigh/CRM framework.

Molecular dynamics (MD) simulations have become a valuable tool for studying the behavior of ESI nano-droplets,[31,44−53] providing information that is difficult to access by experimental approaches.[21−23,26,27] MD simulations have confirmed that small ions such as Na^+ and NH_4^+ are emitted from the nanodroplet surface in accordance with the IEM.[31,32,44,50,53] Clearly, it is desirable to extend these MD approaches to larger analytes. First steps in this direction have been taken recently, when poly ethylene glycol[31] and simplified bead-string protein models[32] were found to behave in accordance with the CEM. Surprisingly, there were only very few attempts to use MD simulations for exploring the behavior of proteins under native ESI conditions.[32,51,52] As a result, it remains uncertain whether the release of protein ions from charged nanodroplets via the CRM represents a viable mechanism.

MD studies of CRM processes have to overcome several challenges. (i) The CRM regime requires long simulation windows because solvent evaporation to dryness is a relatively slow process. The problem is compounded by the fact that the droplets have to be large enough to accommodate macro-molecular analytes. The situation is much more favorable for IEM events, which are rapid (∼1 ns) and thus can be modeled without difficulty.[31,32,44,50,53] (ii) The commonly used approach of running droplet MD simulations at constant energy causes evaporative cooling, which progressively slows down the droplet dynamics.[52,53] Under experimental conditions this cooling is countered by a heated gas environment, and by blackbody radiation emitted from ion source components.[25,54] (iii) ESI usually generates protonated $[M + zH]^{z+}$ ions, with

charge states that are not related to the protein charge in solution.[19,55] Hence, native ESI simulations must include ways to alter the protein charge as the analyte transitions from the droplet into the gas phase. Protonation changes are problematic because standard MD protocols use fixed charges.[56] Simulations involving proton transfer events require QM/MM[57] or ab initio MD approaches[47,58] that are not practical when investigating large systems on long time scales.

In the current work we demonstrate for the first time that MD simulations are capable of providing mechanistic insights into the formation of gaseous protein ions under native ESI conditions. Data are presented for three proteins that have been widely used as ESI-MS model analytes, ubiquitin (Ubq), cytochrome c (Cyt c), and holo-myoglobin (hMb). The native structures of all three species are characterized by a compact globular fold.[59−61] We adopt a trajectory stitching approach that was recently developed for salt cluster ESI simulations,[49] thereby addressing the issues (i) and (ii) outlined above. We sidestep issue (iii) by focusing on sodiated protein ions instead of modeling protonation events. The resulting time-dependent data provide unequivocal support for the view that native ESI converts globular proteins into gaseous ions via the CRM, while preserving a compact analyte structure.

■ METHODS

Proteins and Reagents. Bovine Ubq (neutral mass $M = 8565$ Da), equine heart Cyt c (12359 Da), and equine hMb (17568 Da) were purchased from Sigma (St. Louis, MO). Native solutions were prepared with a protein concentration of 5 μM in 10 mM aqueous ammonium acetate at pH 7. Acidic and basic Ubq solutions were prepared in water containing 2.65 mM formic acid (pH 3) or 70 mM ammonium hydroxide (pH 11.2), respectively.

Mass Spectrometry and Ion Mobility Spectrometry. ESI mass spectra were acquired on a Synapt HDMS mass spectrometer (Waters, Milford, MA) equipped with a Z-spray ESI source. Ion mobility data were recorded using the instrument's traveling-wave IMS cell. Solutions were infused at 5 μL min^{-1}. ESI was carried out at a capillary voltage of +2.8 kV. All potential gradients along the ion path were tuned to be as gentle as possible by maximizing the relative intensity of the most compact IMS conformers. Drift times were converted to collision cross sections (Ω).[62] Ω values of MD structures were calculated using the extended hard sphere scattering method implemented in MOBCAL.[63]

Molecular Dynamics Simulations. MD simulations employed GROMACS 5.0 for leapfrog integration of Newton's equations with a 2 fs time step,[56] using quad core Linux workstations equipped with Nvidia (Santa Clara, CA) graphic processing units (GPUs). Ubq, Cyt c, and hMb were modeled based on crystal structures 1UBQ,[59] 1HRC,[60] and 1WLA,[61] respectively. Solvent molecules were removed, and hydrogens were added using the GROMACS program PDB 2GMX. Unless noted otherwise, we employed TIP4P/2005 water[64] with the CHARMM force field (version 36)[65] modified to include neutral Arg[66] and heme c.[67] CHARMM was chosen because it describes the folding and dynamics of small globular proteins exceedingly well.[65,68] An in-house script was used to build the Cyt c topology, which allowed for iron ligation by His18 and Met80, as well as Cys14/heme and Cys17/heme linkages. Unless noted otherwise, all titratable sites were set to their default pH 7 protonation states. This includes deprotonation of both heme proprionates.

Droplets were built by centering the protein inside a rhombic dodecahedron. This structure was subsequently surrounded by pre-equilibrated water using the GROMACS SOLVATE utility. Spherical droplets were carved by applying a Perl program that removes all molecules that are farther than 3 nm from the protein center of mass. The number of water molecules ranges from ∼3100 for hMb to ∼3500 for Ubq. Random water molecules were replaced with Na^+ to bring the total system charge to 16+. For some simulations the droplets

contained an additional 10 Na$^+$ and 10 Cl$^-$. For each of the various conditions we conducted five MD runs with different initial (random) positions of Na$^+$ and Cl$^-$ and with different initial velocities. Error bars in figures represent standard deviations.

Each droplet was placed in a 1000 nm vacuum box using potential-shifted van der Waals and Coulomb cut-offs of 333.3 nm. Although this configuration technically employs periodic boundary conditions, the parameters used prevent molecules belonging to different replicas from ever interacting with each other. This approach was chosen because it facilitates the implementation of GPU acceleration, which yields greatly reduced run times. Neighbor lists were updated every 50 steps using the Verlet buffer method.[69] All bonds were constrained, using LINCS[70] for proteins and SETTLE[71] for water. The droplets were initially subjected to steepest descent energy minimization, followed by 5 ps of equilibration at the desired temperature.

Production runs were conducted using a recently developed trajectory stitching method.[49] Under this scheme the simulations were broken up into 500 ps windows during which the system was Nosé−Hoover[72] thermalized with a coupling constant of $\tau_T = 0.5$ ps. At the end of each window, any evaporated species that had moved more than 15 nm away from the protein center of mass were removed from the system. The droplet was then recentered in the box, and new velocities were sampled from a Maxwell−Boltzmann distribution prior to beginning the next simulation window. This approach is suitable for stabilizing the temperature of evaporating droplets over long trajectories with deviations of no more than ±5%,[49] thereby eliminating evaporative cooling problems. Trajectory stitching has the additional benefit of reducing the number of particles over the course of the simulation, resulting in considerable time savings. The periodic reinitialization of particle velocities mimics the thermal environment (heated gas and blackbody radiation field)[25,54] experienced under experimental conditions. For very small systems a gas bath can be simulated explicitly,[48] but for the size range considered here the computational cost becomes prohibitive, making approaches such as the one used the preferred choice.[73] Unless noted otherwise, the simulations were run at 370 K for 75 ns. After this period the temperature was increased to 450 K for 50 ns to promote the final stages of solvent evaporation. This temperature increase reflects progressive heating as protein ions traverse the declustering region and subsequent ion optics of the mass spectrometer.[25,74,75]

RESULTS AND DISCUSSION

Native ESI-MS and IMS Experiments. Prior to discussing MD results it is instructive to have a look at the [M + zH]$^{z+}$ ions produced experimentally for Ubq, Cyt *c*, and hMb under native ESI conditions. The mass spectrum of Ubq is dominated by the 6+ charge state. The Cyt *c* data show prominent 7+ and 8+ signals, whereas the highest intensity peak in the hMb spectrum corresponds to 9+ ions. As expected,[20,34] these charge states are close to the z_R values predicted by eq 1 for a protein density of 1 g cm^{-3} (6.6+, 7.9+, and 9.5+, Figure 1A−C). Ion mobility spectra show well-resolved peaks that signify the presence of relatively uniform gas phase conformations (Figure 1D−F). The measured Ω values of 1010, 1380, and 1820 Å^2 are in agreement with previous native ESI-IMS studies.[7,76,77]

Protonated vs Sodiated Gas Phase Proteins. It is usually desirable to operate under ESI conditions that produce [M + zH]$^{z+}$ ions, but analyte charging can also be mediated by species other than protons. The presence of sodium acetate favors the formation of mixed protonated/sodiated protein ions. The charge state distribution of these ions is unchanged relative to the conditions of Figure 1. Also, ions ranging from [M + zH]$^{z+}$ to [M + zNa]$^{z+}$ exhibit virtually the same collision cross sections (Supporting Figure S1).

The similarities in charge states and collision cross sections suggest that the formation mechanisms of protonated and sodiated gas phase proteins share many common features. This
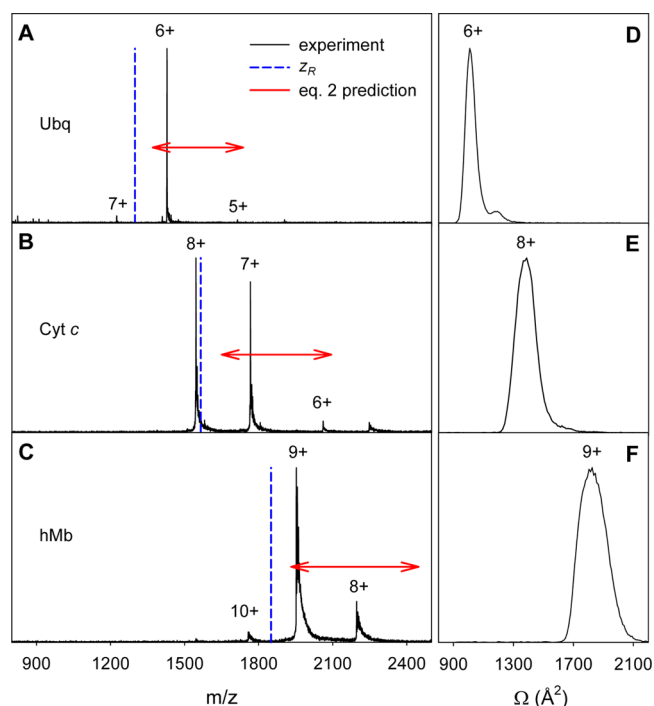

Figure 1. ESI mass spectra of (A) Ubq, (B) Cyt *c*, and (C) hMb recorded at pH 7 in aqueous solution. Also shown are the Rayleigh z_R values, calculated using eq 1 (blue), and the charge state range predicted by eq 2 (red). (D−F) display IMS distributions of the three proteins.

assertion has major implications for the viability of native ESI simulations. Obstacles associated with MD studies on [M + zH]$^{z+}$ ions have been noted above.[47,57,58] In this work we adopt an approach that employs Na$^+$ as surrogate charge carrier, rather than focusing on H$^+$. Unlike protonation, metal cation binding to proteins is governed by Coulombic and van der Waals interactions[35,78] that are well described by standard MD force fields.[49,56,65] Accordingly, the simulation strategy used here places proteins in aqueous droplets that are charged with excess Na$^+$. It is indeed possible to devise ESI sources that produce aqueous droplets with an excess charge that is entirely due to Na$^+$,[79] analogous to the simulated systems considered here. We could have picked a different type of monatomic cation for our simulations; our choice of Na$^+$ reflects the fact that sodium salts are commonly encountered in biological samples.

Native ESI Simulations Using Na$^+$ Containing Droplets. ESI simulations were conducted by initially placing a natively folded protein in the center of an aqueous droplet with 3 nm radius. Excess Na$^+$ were included to bring the total system charge to 16+, corresponding to 86% of the Rayleigh limit. This total charge includes all contributions from protein side chains and termini expected for pH 7, keeping in mind that the goal of this work is to simulate the ESI process under native solvent conditions. The protein intrinsic charge is zero for Ubq, 6+ for Cyt *c*, and 2- for hMb. The corresponding ESI droplets therefore initially contained 16, 10, and 18 Na$^+$, respectively.

Figure 2A−F illustrates snapshots taken from a typical Ubq trajectory. Panel A shows the protein within the equilibrated ESI droplet, surrounded by water and Na$^+$. Solvent evaporation gradually reduces the droplet size. This shrinkage is accompanied by the occasional ejection of solvated Na$^+$ (Figure 2B). These Na$^+$ ejection events are well described by the
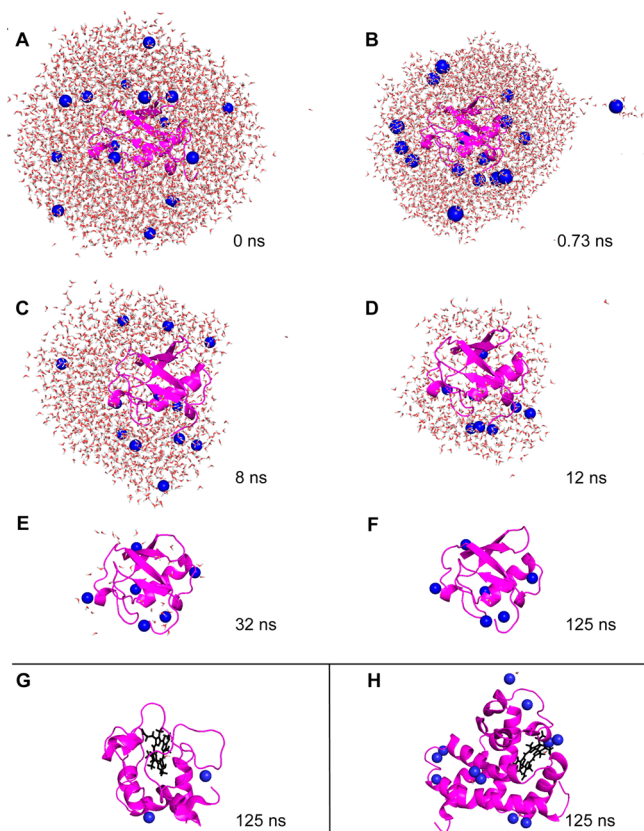
Figure 2. MD simulation snapshots of aqueous nanodroplets with an initial 3 nm radius containing Na⁺ and a 16+ overall charge. (A–F) ESI process of Ubq. (G) Final (125 ns) MD frame of the Cyt *c* ESI process. (H) Final MD frame of the hMb ESI process. The protein backbone is shown in magenta, heme is black, water oxygen is red, Na⁺ is blue.

IEM.[28,32,44] Na⁺ ions within the droplet initially behave as freely dissolved species, but they start to interact with the protein surface as solvent evaporation proceeds (Figure 2D, E). After 125 ns the protein is completely solvent-free and bears six Na⁺, corresponding to a gaseous $[M + 6Na]^{6+}$ ion. Many of the metal-protein interactions are mediated by carboxylates (Asp⁻ and Glu⁻ side chains, C-terminus⁻). In addition, some backbone and side chain carbonyls are in contact with metal ions. Binding motifs of this type are well established in the literature.[35,78] Two Na⁺ are part of surface clusters that involve Lys⁺ side chains (Supporting Figure S2A).

MD trajectories similar to those discussed for Ubq were observed for Cyt *c* and hMb (SI Movies). Gaseous product structures obtained for these two proteins are exemplified in Figure 2G, H. The corresponding final ion compositions are $[M + 6H + 2Na]^{8+}$ for Cyt *c*, and $[M − 2H + 11Na]^{9+}$ for hMb. Surplus or missing protons arise from the pH 7 titration behavior, as explained above

Native ESI Simulations in the Presence of NaCl. Nonvolatile salts interfere with native ESI-MS by promoting the formation of heterogeneous adducts. NaCl is particularly notorious due to its tendency to generate $[M + zH + n(Na − H) + m(Cl + H)]^{z+}$ ions.[35] Adduct formation does not affect ESI charge states[80] (exemplified in Supporting Figure S3). To examine the mechanism of adduction we conducted ESI simulations in the presence of 10 Na⁺ and 10 Cl⁻ (in addition to the Na⁺ excess charge carriers). For the droplets considered

here 10 NaCl correspond to a concentration of 0.15 M. This is higher than the salt content of typical analyte solutions, but it reflects the fact that solute concentrations in ESI droplets are increased by solvent evaporation.[20,49]

The ESI process for Ubq in a Na⁺/NaCl droplet is illustrated in Figure 3A–F. Consistent with earlier data,[49] Coulombic
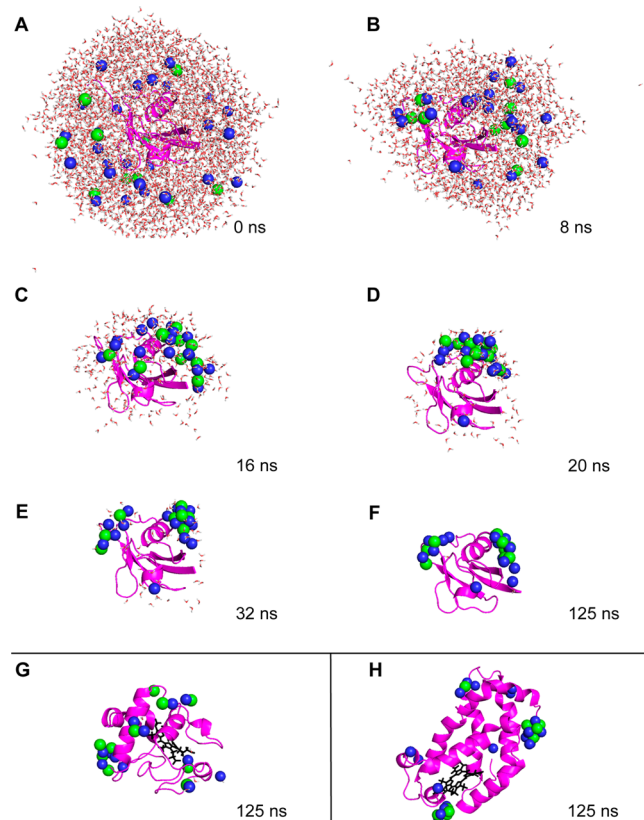

Figure 3. MD simulation of the ESI process as in Figure 2, but in the presence of NaCl. (A–F) Evaporation of a Ubq containing droplet. The final frames of Cyt *c* and hMb ESI simulations are shown in (G) and (H), respectively. Element coloring is as in Figure 2; Cl⁻ is shown in green.

attraction prevents the ejection of Cl⁻ from the positively charged droplet, while Na⁺ emission proceeds in an IEM fashion as noted above. As the droplet gradually dries the remaining Na⁺ and Cl⁻ start to crowd around the protein (Figure 3C). Upon further water loss most of the salt ions separate into two clusters that attach to the protein surface (Figure 3E, F). The formation of these protein-bound salt clusters is surprising. Earlier proposals had envisioned the formation of a more evenly distributed "salt crust" formed by ion pairing of individual Na⁺ and Cl⁻ with charged side chains.[35] The desolvated ESI product in Figure 3F has the composition $[M + 16Na + 10Cl]^{6+}$. Anchoring of salt clusters at the protein surface is provided mainly by carboxylates, aided by Arg⁺ and Lys⁺ side chains, as well as backbone carbonyls and other polar contacts (Supporting Figure S2B). ESI scenarios very similar to these Ubq data were observed for the other two proteins in Na⁺/NaCl droplets (see SI Movies). Figure 3G,H exemplifies two of the product ions, i.e., $[M + 6H + 12Na + 10Cl]^{8+}$ for Cyt *c*, and $[M − 2H + 21Na + 10Cl]^{9+}$ for hMb.

Comparing MD Results and Experimental Data. MD simulations were run for all three proteins, using Na⁺ charged

droplets with and without NaCl. Gratifyingly, the charge states obtained in these simulations show excellent agreement with the experimental data (Figure 4A). Collision cross sections of
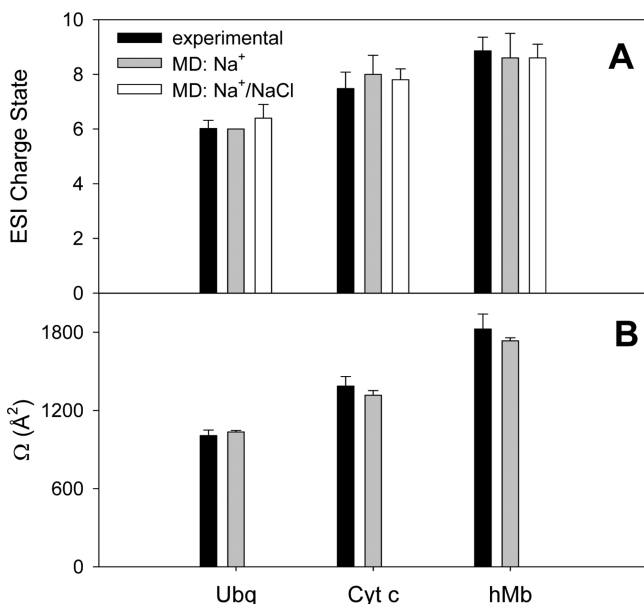

Figure 4. (A) Experimental ESI charge states compared with MD simulation results for Ubq, Cyt *c*, and hMb. MD results are shown for droplets containing Na$^+$, as well as Na$^+$/NaCl. (B) Experimental collision cross sections with their half-widths compared to MD structures. Simulation data represent the final (125 ns) configurations of five independent runs.

the MD structures are in close agreement with the experimental Ω values as well (Figure 4B). Results for Na$^+$/NaCl simulations are not included in Figure 4B because it is difficult to conduct ion mobility measurements on NaCl-adducted protein ions due to S/N limitations.

Native ESI: A CRM Process. The key question explored here is whether native ESI produces gaseous proteins via the CRM,[20,30,32−34] the IEM,[40,81] or by some other mechanism.[31,32,36,41,42] Figures 2 and 3 demonstrate that desolvated protein ions are formed by solvent evaporation to dryness, which represents the hallmark of the CRM.[20,30,32−34] This point is further illustrated in Figure 5 which displays the protein center of mass (COM) relative to the water COM. It is seen that the protein COM always stays well within the droplet interior. This behavior is *not* consistent with the IEM (or the CEM) where analytes are ejected from the droplet surface.[31,32,40,81] Instead, under native ESI conditions a "charged residue" of nonvolatile moieties (protein, charge carriers, and salt) is left behind as the final solvent layers evaporate. On the basis of these morphological features,[20,30] it is concluded that native ESI proceeds according to the CRM.

The crystal structures of native Cyt *c* and hMb reveal a typical globular fold with a hydrophobic core, while most charged and polar side chains are on the protein surface.[60,61] This hydrophilic exterior has a strong tendency to remain solvated by water, such that protein positions within the droplet interior are preferred (Figure 5B, C).[32] Interestingly, Ubq prefers off-center positions within the droplet. This is seen in Figure 5A, which shows larger radial positions than for the other two proteins. Ubq has a patch of nonpolar surface residues (L8, I36, P37, I44, V70, L71, and L73).[59] The Ubq
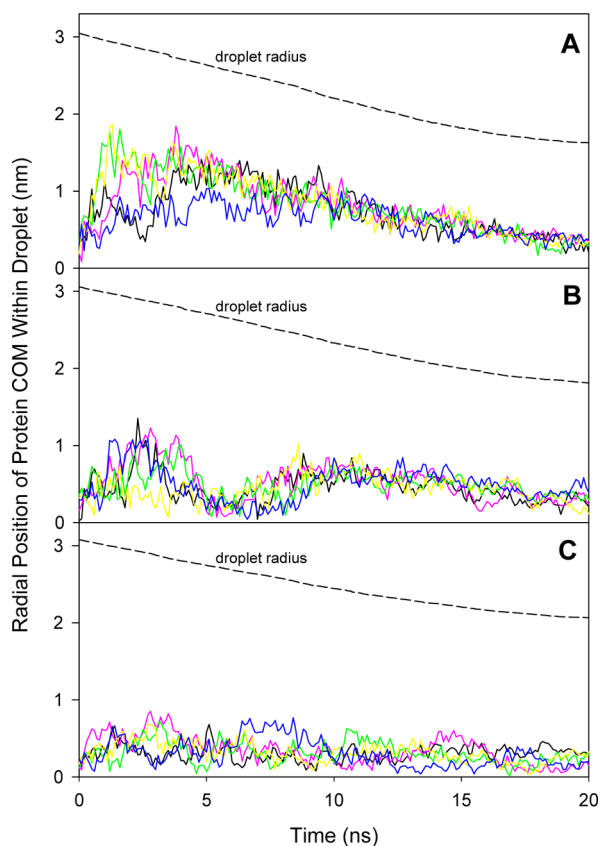

Figure 5. Position of (A) Ubq, (B) Cyt *c*, and (C) hMb within the shrinking ESI droplet. Each panel shows five MD runs using Na$^+$ charged droplets without additional NaCl. Data were generated by calculating the difference between protein center of mass (COM) and water COM. Also shown is the droplet radius, which indicates the position of the liquid/vapor interface relative to the droplet center. The 20 ns time window shown here accounts for >95% solvent loss.

preference for off-center positions reflects the tendency of these hydrophobic sites to minimize water contact, which is achieved by having them protrude from the surface (Figure 2C, Supporting Figure S4). CRM depictions often show the protein at the droplet center.[4,32] This is adequate for some proteins, but not for others. Our Ubq data demonstrate that the CRM can also take place while the protein resides close to the surface.

Protein Charging During Native ESI. Figure 6 highlights details of a typical Ubq trajectory. Similar data were obtained for Cyt *c* and hMb (Supporting Figures S5, S6). Solvent evaporation during the initial 20 ns reduces the water content of the system from ~3500 to a few dozen H$_2$O. These last solvent molecules interact with the protein quite strongly, causing the final evaporation steps to be slow (Figure 6A, B). Droplet shrinkage is accompanied by sequential Na$^+$ ejection (Figure 6C). This charge loss comes to a halt when most of the solvent has vanished, triggering binding of the residual Na$^+$ to the protein. The ESI charge state of the CRM product is equal to the number of these adsorbed Na$^+$, plus the intrinsic protein charge (6 + 0 = 6 for Ubq, 2 + 6 = 8 for Cyt *c*, and 11 + (−2) = 9 for hMb, Figures 6C, S5C, S6C).

What factor determines the number of these residual Na$^+$? The droplet evolution proceeds with a recurring pattern, where solvent loss causes a gradual increase of z/z_R, until a sudden decrease marks the ejection of a Na$^+$ (Figure 6D). The resulting
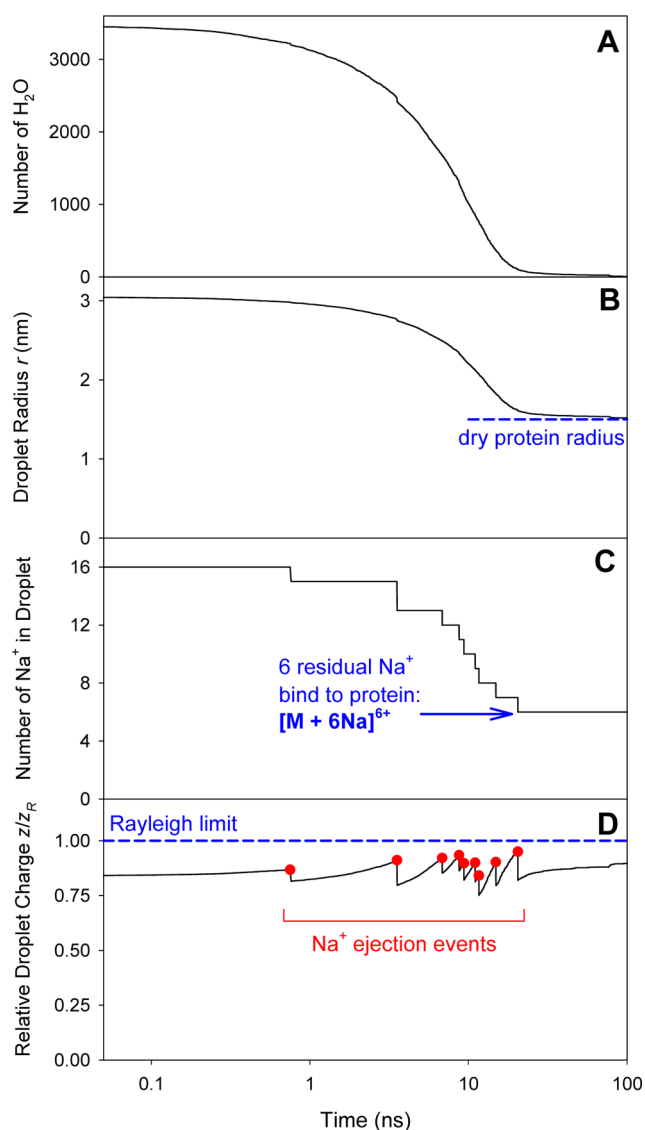
Figure 6. Time-dependent changes in droplet size and charge as a function of time for a Ubq ESI simulation without NaCl. (A) Number of water molecules. (B) Effective radius of the droplet, calculated as[34] $r = 3/4(M\pi^{-1}d^{-1})^{1/3}$ where M is the total mass and $d = 1$ g cm^{-3}. (C) Number of Na$^+$ in the droplet. (D) Total droplet charge relative to the Rayleigh limit eq 1. Red symbols highlight Na$^+$ ejection events. Note that the time axis is logarithmic.

sawtooth-like profile is reminiscent of data obtained experimentally for larger droplets.[22] The shrinkage/ejection cycle repeats itself until the droplet has dried out. The number of residual Na$^+$ is governed by the fact that the relative droplet charge z/z_R is confined to the range of roughly 0.85 ± 0.1. Values of z/z_R beyond 0.95 are prevented by IEM ejection of Na$^+$,[31,32,44,50,53] which functions as an electrostatic "stress relief valve". Thus, protein ions in native ESI are formed via the CRM, while the IEM plays an ancillary role by governing the overall charge on the shrinking droplet.[38,39,49]

The scenario emerging from Figure 6 can be summarized as follows: the shrinking droplet continuously sheds charge, maintaining z/z_R around 0.85. The charge state of the resulting protein ion depends on the protein size (horizontal line in Figure 6B). For small proteins the droplet will shrink to a small radius r before all the solvent has evaporated. The resulting

droplet charge $z \approx 0.85 \times z_R$ is relatively low, as dictated by the $z_R(r)$ dependence in eq 1. Any Na$^+$ that were not ejected prior to disappearance of the solvent will bind to the protein. For large proteins solvent evaporation comes to a halt at a larger value of r, simply because droplet shrinkage must stop once the dry protein surface is exposed. The vanishing droplet will carry a larger droplet charge z, resulting in a higher ESI charge state. The dependence of z on protein size is illustrated by the data of this work, i.e., Ubq (6+) < Cyt c (8+) < hMb (9+). This mechanism explains why native ESI charge states are related to the protein surface area.[82] These data provide the first molecular-level verification of the Rayleigh/CRM framework, according to which the protein charge in native ESI is equal to that of a protein-sized water droplet slightly below z_R.[20,34] Overall, native ESI converts globular proteins into gaseous ions with charge states that cover the range of approximately

$$0.75 z_R < z_{\text{protein}} < 0.95 z_R \qquad (2)$$

where z_R is given by eq 1, with an effective protein radius r calculated for a density of[34] 1 g cm^{-3}. Figure 1A−C demonstrates that this relationship predicts the experimental ESI charge states of Ubq, Cyt c, and hMb remarkably well. The same is true for a wide range of other proteins.[20,34]

Robustness of the Rayleigh/CRM Framework. Focusing on Ubq as test system, we explored to what extent the simulation results depend on specific parameters and model assumptions. We initially verified that the results obtained are valid for different force fields, as demonstrated by a CHARMM36[65] vs OPLS/AA[83] comparison (Figure 7A).

Another question is related to the charges on side chains and termini. The use of pH 7 titration values for the simulations above reflects the view that most solution charges are retained in the gas phase.[35,37,51] On the other hand, it is possible that this zwitterionic character is lost due to intramolecular proton transfer (e.g., Lys$^+$ + Glu$^-$ → Lys^0 + Glu^0) at some point during ESI.[76] For exploring this issue we also conducted simulations on all-neutral Ubq (N-terminus^0, Arg^0, Lys^0, Glu^0, Asp^0, C-terminus^0). The ESI process under these conditions is very similar to that of Figure 2. However, the binding of residual Na$^+$ and Cl$^-$ is mediated by backbone and side chain carbonyls, as well as other polar contacts (Supporting Figure S7). This is different from the zwitterionic scenario, where numerous contacts were formed by carboxylates (Supporting Figure S2). In the absence of NaCl the zwitterionic scenario results in an average ESI charge state of 6+, whereas a value of 5+ was generated under all-neutral conditions. In the presence of NaCl the ESI charge state was identical for both scenarios (6+, Figure 7B). It is concluded that the native ESI mechanism and the resulting protein charge states are not very sensitive to the titration behavior of the protein. This finding is reassuring, keeping in mind that the charge pattern under ESI conditions is difficult to predict.[37,76]

It is occasionally suggested that the Rayleigh/CRM framework eq 2 is only viable under conditions where the initial protein net charge is zero.[41] Ubq is a good test system for addressing this point, because its solution charge can be modulated over a wide range while leaving the native structure intact.[59,84] Ubq has a net charge of zero at neutral pH, while producing 6+ ions during ESI. Upon raising the pH to 11.2 the solution charge decreases to 9−, but the ESI charge remains at 6+. At pH 3 the solution charge is 12+, while the ESI mass spectrum shows a slight shift to 7+ (Supporting Figure S8). MD simulations were conducted to explore the effects of the
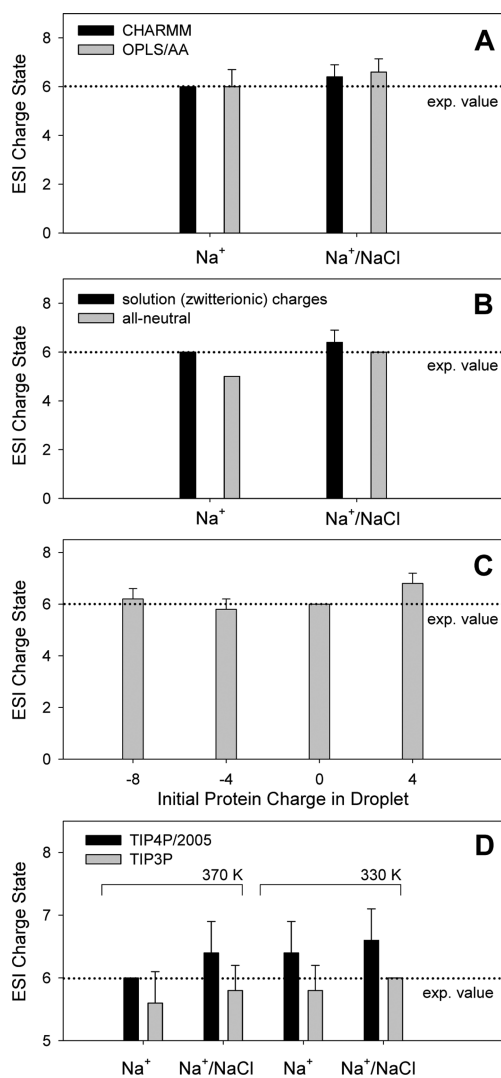
Figure 7. ESI charge states for Ubq generated under various MD conditions. Unless noted otherwise, TIP4P/2005 water and pH 7 solution charges were used. Results are shown for droplets containing Na$^+$, as well as Na$^+$/NaCl. (A) MD results for different force fields. (B) Comparison of pH 7 charges on side chains and termini vs all-neutral. (C) Results obtained for different initial protein net charge values. For "0" all sites had their pH 7 charges. The following sites were neutralized for implementing different initial charge states: 4+, E16, E24, E34, E64; 4-, K11, K29, K48, K63; 8- N-terminus, K6, K11, K27, K29, K33, K48, K63. (D) Comparison of TIP4P/2005 and TIP3P water at different initial temperatures.

initial net protein charge, testing the range from 4+ to 8− by manually modifying selected residues (see caption of Figure 7C for details). In each case excess Na$^+$ were added to ensure a total droplet charge up to 16+. Droplet evaporation and protein release proceeded as in Figure 2. Initial protein charges of zero down to 8− all produced gaseous 6+ ions. For an initial 4+ protein charge the MD charge state increased slightly to 6.8. These simulation results are consistent with the experimental finding that ESI charge states are largely independent of the net protein charge in solution, as long as the native conformation remains intact.[19] The observed behavior is a natural consequence of the Rayleigh/CRM framework, because in each case the *total* droplet charge (including the protein charge) remains at ∼0.85 z_R. As a consequence, 6 Na$^+$ will be available for binding to Ubq^0 when the solvent vanishes, while

14 Na$^+$ will be available for Ubq^{8-}. In both cases the CRM produces gaseous Ubq^{6+} (Figure 7C). In other words, there are no unresolved issues when applying the Rayleigh/CRM framework to conditions where pH ≠ pI.

The Rayleigh/CRM framework predicts that it should be possible to modulate ESI charge states by changing the surface tension.[33] Lower values of γ are expected to reduce analyte z values because the shrinking droplets will not be able to hold as much charge eq 1. This prediction can be tested by using different water models. The simulations discussed above employed TIP4P/2005 water which reproduces the experimental γ to within a ∼ 1%. TIP3P water provides a much lower γ (0.039 vs 0.057 N m^{-1} at 370 K).[85] TIP3P simulations consistently yielded lower ESI charge states than TIP4P/2005 runs (Figure 7D). On average, the charge state ratio for the two models is 0.91. This effect is somewhat less pronounced than expected from the surface tension values, where (γ_{TIP3P}/$\gamma_{TIP4P/2005}$)$^{1/2}$ = 0.83. The validity of the model is nonetheless supported by the fact that the MD simulations reproduce the expected $z(\gamma)$ trend.

Structure Retention in the Gas Phase. RMSD plots were generated to track changes in protein structure during ESI, using crystal data as reference. During equilibration the RMSDs rise to around 0.1 nm. In NaCl-free droplets this is followed by an increase to values around 0.3 to 0.4 nm. For Ubq this transition is gradual, whereas the RMSD profiles of Cyt c and hMb show a behavior that is more step-like (Figure 8A−C). The first of these steps takes place after ∼20 ns, when most of the water has evaporated (cf. Figure 6). The second step coincides with the temperature increase from 370 to 450 K which was implemented for promoting the final desolvation events. The overall magnitude of these structural changes is quite modest. Overlays of the final MD conformations with the corresponding crystal structures confirms that all proteins retain a native-like compactness. Secondary and tertiary structure are largely preserved, although some helices, strands, loops and termini undergo moderate changes in orientation (Figure 8D− F). The collision cross sections of these MD structures agree well with experimental Ω values (Figure 4B).

ESI simulations on Na$^+$/NaCl droplets reveal a high degree of structure retention for Ubq and Cyt c. Conformational distortion is more pronounced for NaCl-bound hMb, where final RMSDs approach 0.5 nm in two of the runs (Supporting Figure S9). Hence, the binding of charged salt clusters to gaseous proteins (Figure 3F−H) can promote the occurrence of structural changes to a larger extent than the spread-out binding of individual Na$^+$ (Figure 2F−H).

■ CONCLUSIONS

The MD simulations of this work provide the first atomistic view of protein release from highly charged ESI droplets into the gas phase. We focus on native ESI conditions, where the protein adopts a tightly folded, globular structure when the process commences. On the basis of morphological features (solvent evaporation to dryness)[20,30] it is concluded that ESI proceeds according to the CRM. Proteins with a hydrophobic core and a hydrophilic exterior remain close to the droplet center, governed by the tendency of polar and charged side chains to stay solvated as long as possible. In contrast, proteins with exposed hydrophobic sites reside at the (inside) droplet surface. Both cases represent viable CRM scenarios. An interesting finding is the formation of salt clusters on the protein surface when conducting ESI in the presence of NaCl.
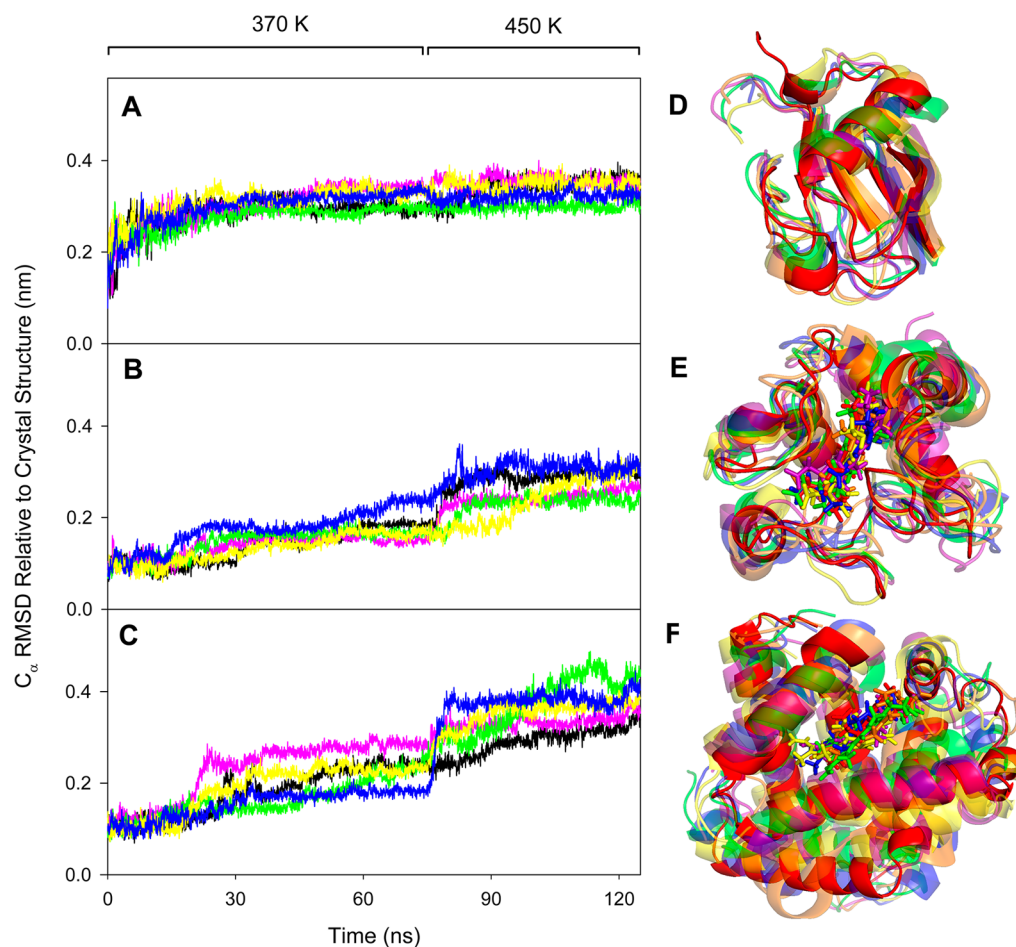
Figure 8. RMSD values of (A) Ubq, (B) Cyt *c*, (C) hMb relative to crystal C_α positions during droplet simulations in the absence of NaCl. Data for different runs are displayed in different colors. (D−F) show overlays of the corresponding final (*t* = 125 ns) conformations, with the crystal structure included in red. The simulation temperature profile is indicated along the top.

This contrasts earlier suggestions of adduct formation in a spread-out fashion.[35] We reiterate that the current study deals with folded proteins. Unfolded chains likely do not follow the CRM,[4,32] requiring the implementation of different all-atom MD strategies that will be explored elsewhere.

Classification of native ESI as a CRM process does not have any per se implications for the mechanism of analyte charging. However, close examination reveals that our trajectories provide direct support for the Rayleigh model,[20,34] which envisions that the relative droplet charge is pegged at around $C \times z_R$, with $C \approx 0.85$ for the conditions used here. As suggested previously,[38,39,49] we find that the droplet charge is governed by the IEM ejection of small ions during shrinkage. Ultimately, the evaporating droplet morphs into a dried-out protein. At this point the residual charge carriers are transferred to the protein surface. All considerations within this Rayleigh/CRM framework refer to the *total* charge, including the protein intrinsic charge as well as excess ions. It is remarkable that the Rayleigh/CRM framework quite accurately predicts the ESI charge states of globular proteins regardless of the physicochemical properties of the analyte. The only pertinent variables are the effective protein radius *r* and the surface tension *γ*. Changes in both of these parameters produce the expected trends in our simulations.

A competing proposal envisions that protein charge states in native ESI are determined by apparent gas phase basicities, i.e.,

by microscopic details of H⁺/protein interactions.[37,43] However, identical charge states are observed for protonated and sodiated proteins. More importantly, the mode of charge carrier binding (via charged or neutral side chains, with Cl⁻ or without) has only minor effects on the ESI charge state. These findings imply that *proton* affinity is not a major factor for governing the outcome of the process under native ESI conditions. Instead, ESI charge states are governed primarily by the ability of the shrinking droplets to hold on to their excess ions, as envisioned by the Rayleigh/CRM framework.

The conclusion that ESI droplets evolve with a total charge of roughly $C \times z_R$ (where $C \approx 0.85$) was reached here for aqueous systems with an excess positive charge due to the presence of monatomic ions. We do not claim that the same value of C applies to every other solvent, every other type of charge carrier, or for droplets with negative polarity. It is well established that nonaqueous solvents can show different stabilities,[22] and that other types of ions give rise to different charge retention.[80] Such factors have to be carefully considered when designing experiments aimed at scrutinizing the validity of ESI mechanisms.[39,42] Instrumental factors can also modulate protein charge states to some extent, such that the agreement between theory and experiment may not always be perfect.[19] Such deviations may require minor modifications of the Rayleigh/CRM framework, rather than pointing to fundamental flaws of the underlying ideas.

Our simulations confirm that nascent protein ions produced by native ESI retain much of their solution structure. At least on the time scale considered here there is no evidence of large-scale conformational changes, such as the formation of "inside-out" conformers that may represent the lowest free energy state in the gas phase.[14] It cannot ruled out, however, that such structural changes will take place on longer time scales, particularly when the gaseous proteins experience thermal activation that may help overcome barriers on their energy landscapes.[86] Nonetheless, the findings of this study support the view that the interrogation of electrosprayed protein ions provides insights that are pertinent to the protein behavior in solution. This conclusion has profound implications for the rapidly growing number of research initiatives in an area that is often referred to as "gas phase structural biology".

■ ASSOCIATED CONTENT

Ⓢ Supporting Information

The Supporting Information is available free of charge on the ACS Publications website at DOI: 10.1021/jacs.5b07913.

Figures S1−S9. (PDF)
Movie S1. (MPG)
Movie S2. (MPG)
Movie S3. (MPG)
Movie S4. (MPG)
Movie S5. (MPG)
Movie S6. (MPG)

■ AUTHOR INFORMATION

Corresponding Author

*konerman@uwo.ca

Notes

The authors declare no competing financial interest.

■ ACKNOWLEDGMENTS

■ REFERENCES

(1) Fenn, J. B. *Angew. Chem., Int. Ed.* **2003**, *42*, 3871−3894.
(2) Muneeruddin, K.; Thomas, J. J.; Salinas, P. A.; Kaltashov, I. A. *Anal. Chem.* **2014**, *86*, 10692−10699.
(3) Heck, A. J. R. *Nat. Methods* **2008**, *5*, 927−933.
(4) Mehmood, S.; Allison, T. M.; Robinson, C. V. *Annu. Rev. Phys. Chem.* **2015**, *66*, 453−474.
(5) Young, L. M.; Saunders, J. C.; Mahood, R. A.; Revill, C. H.; Foster, R. J.; Tu, L.-H.; Raleigh, D. P.; Radford, S. E.; Ashcroft, A. E. *Nat. Chem.* **2015**, *7*, 73−81.
(6) Silveira, J. A.; Servage, K. A.; Gamage, C. M.; Russell, D. H. *J. Phys. Chem. A* **2013**, *117*, 953−961.
(7) Wyttenbach, T.; Bowers, M. T. *J. Phys. Chem. B* **2011**, *115*, 12266−12275.
(8) Bohrer, B. C.; Merenbloom, S. I.; Koeniger, S. L.; Hilderbrand, A. E.; Clemmer, D. E. *Annu. Rev. Anal. Chem.* **2008**, *1*, 293−327.
(9) Ly, T.; Julian, R. R. *J. Am. Chem. Soc.* **2010**, *132*, 8602−8609.
(10) Liu, L.; Bagal, D.; Kitova, E. N.; Schnier, P. D.; Klassen, J. S. *J. Am. Chem. Soc.* **2009**, *131*, 15980−15981.
(11) Warnke, S.; Baldauf, C.; Bowers, M. T.; Pagel, K.; von Helden, G. *J. Am. Chem. Soc.* **2014**, *136*, 10308−10314.
(12) Shaw, J. B.; Li, W.; Holden, D. D.; Zhang, Y.; Griep-Raming, J.; Fellers, R. T.; Early, B. P.; Thomas, P. M.; Kelleher, N. L.; Brodbelt, J. S. *J. Am. Chem. Soc.* **2013**, *135*, 12646−12651.
(13) Mikhailov, V. A.; Mize, T. H.; Benesch, J. L. P.; Robinson, C. V. *Anal. Chem.* **2014**, *86*, 8321−8328.
(14) Wolynes, P. G. *Proc. Natl. Acad. Sci. U. S. A.* **1995**, *92*, 2426−2427.
(15) Silveira, J. A.; Fort, K. L.; Kim, D.; Servage, K. A.; Pierson, N. A.; Clemmer, D. E.; Russell, D. H. *J. Am. Chem. Soc.* **2013**, *135*, 19147−19153.
(16) van der Spoel, D.; Marklund, E. G.; Larsson, D. S. D.; Caleman, C. *Macromol. Biosci.* **2011**, *11*, 50−59.
(17) Ruotolo, B. T.; Robinson, C. V. *Curr. Opin. Chem. Biol.* **2006**, *10*, 402−408.
(18) Bich, C.; Baer, S.; Jecklin, M. C.; Zenobi, R. *J. Am. Soc. Mass Spectrom.* **2010**, *21*, 286−289.
(19) Kaltashov, I. A.; Abzalimov, R. R. *J. Am. Soc. Mass Spectrom.* **2008**, *19*, 1239−1246.
(20) Kebarle, P.; Verkerk, U. H. *Mass Spectrom. Rev.* **2009**, *28*, 898−917.
(21) Gomez, A.; Tang, K. *Phys. Fluids* **1994**, *6*, 404−414.
(22) Grimm, R. L.; Beauchamp, J. L. *J. Phys. Chem. A* **2010**, *114*, 1411−1419.
(23) Taflin, D. C.; Ward, T. L.; Davis, E. J. *Langmuir* **1989**, *5*, 376−384.
(24) Lide, D. R. *CRC Handbook of Chemistry and Physics*, 82nd ed.; CRC Press: Boca Raton, FL, 2001.
(25) Covey, T. R.; Thomson, B. A.; Schneider, B. B. *Mass Spectrom. Rev.* **2009**, *28*, 870−897.
(26) Arscott, S.; Descatoire, C.; Buchaillot, L.; Ashcroft, A. E. *Appl. Phys. Lett.* **2012**, *100*, 074103.
(27) Nemes, P.; Marginean, I.; Vertes, A. *Anal. Chem.* **2007**, *79*, 3105−3116.
(28) Iribarne, J. V.; Thomson, B. A. *J. Chem. Phys.* **1976**, *64*, 2287−2294.
(29) Loscertales, I. G.; de la Mora, J. F. *J. Chem. Phys.* **1995**, *103*, 5041−5060.
(30) Dole, M.; Mack, L. L.; Hines, R. L.; Mobley, R. C.; Ferguson, L. D.; Alice, M. B. *J. Chem. Phys.* **1968**, *49*, 2240−2249.
(31) Consta, S.; Oh, M. I.; Soltani, S. *Int. J. Mass Spectrom.* **2015**, *377*, 557−567.
(32) Konermann, L.; Ahadi, E.; Rodriguez, A. D.; Vahidi, S. *Anal. Chem.* **2013**, *85*, 2−9.
(33) Iavarone, A. T.; Williams, E. R. *J. Am. Chem. Soc.* **2003**, *125*, 2319−2327.
(34) de la Mora, F. J. *Anal. Chim. Acta* **2000**, *406*, 93−104.
(35) Verkerk, U. H.; Kebarle, P. *J. Am. Soc. Mass Spectrom.* **2005**, *16*, 1325−1341.
(36) Ogorzalek Loo, R. R.; Lakshmanan, R.; Loo, J. A. *J. Am. Soc. Mass Spectrom.* **2014**, *25*, 1675−1693.
(37) Li, J.; Santambrogio, C.; Brocca, S.; Rossetti, G.; Carloni, P.; Grandori, R. *Mass Spectrom. Rev.* **2015**, DOI: 10.1002/mas.10044.
(38) Hogan, C. J.; Carroll, J. A.; Rohrs, H. W.; Biswas, P.; Gross, M. L. *Anal. Chem.* **2009**, *81*, 369−377.
(39) Allen, S. J.; Schwartz, A. M.; Bush, M. F. *Anal. Chem.* **2013**, *85*, 12055−12061.
(40) Nguyen, S.; Fenn, J. B. *Proc. Natl. Acad. Sci. U. S. A.* **2007**, *104*, 1111−1117.
(41) Testa, L.; Brocca, S.; Grandori, R. *Anal. Chem.* **2011**, *83*, 6459−6463.
(42) Samalikova, M.; Grandori, R. *J. Am. Chem. Soc.* **2003**, *125*, 13352−13353.
(43) Schnier, P. D.; Gross, D. S.; Williams, E. R. *J. Am. Soc. Mass Spectrom.* **1995**, *6*, 1086−1097.
(44) Znamenskiy, V.; Marginean, I.; Vertes, A. *J. Phys. Chem. A* **2003**, *107*, 7406−7412.
(45) Mason, P. E.; Uhlig, F.; Vanek, V.; Buttersack, T.; Bauerecker, S.; Jungwirth, P. *Nat. Chem.* **2015**, *7*, 250−254.
(46) Hub, J. S.; Wolf, M. G.; Caleman, C.; Maaren, P. J.; Groenhof, G.; van der Spoel, D. *Chem. Sci.* **2014**, *5*, 1745−1749.
(47) Iyengar, S. S.; Day, T. J. F.; Voth, G. A. *Int. J. Mass Spectrom.* **2005**, *241*, 197−204.

(48) Daub, C. D.; Cann, N. M. *Anal. Chem.* **2011**, *83*, 8372−8376.

(49) Konermann, L.; McAllister, R. G.; Metwally, H. *J. Phys. Chem. B* **2014**, *118*, 12025−12033.

(50) Higashi, H.; Tokumi, T.; Hogan, C. J.; Suda, H.; Seto, T.; Otani, Y. *Phys. Chem. Chem. Phys.* **2015**, *17*, 15746−15755.

(51) Patriksson, A.; Marklund, E.; van der Spoel, D. *Biochemistry* **2007**, *46*, 933−945.

(52) Steinberg, M. Z.; Breuker, K.; Elber, R.; Gerber, R. B. *Phys. Chem. Chem. Phys.* **2007**, *9*, 4690−4697.

(53) Caleman, C.; van der Spoel, D. *Phys. Chem. Chem. Phys.* **2007**, *9*, 5105−5111.

(54) Gibson, S. C.; Feigerle, C. S.; Cook, K. D. *Anal. Chem.* **2014**, *86*, 464−472.

(55) Wang, G.; Cole, R. B. *Org. Mass Spectrom.* **1994**, *29*, 419−427.

(56) Pronk, S.; Pall, S.; Schulz, R.; Larsson, P.; Bjelkmar, P.; Apostolov, R.; Shirts, M. R.; Smith, J. C.; Kasson, P. M.; van der Spoel, D.; Hess, B.; Lindahl, E. *Bioinformatics* **2013**, *29*, 845−854.

(57) Goyal, P.; Qian, H. J.; Irle, S.; Lu, X. Y.; Roston, D.; Mori, T.; Elstner, M.; Cui, Q. *J. Phys. Chem. B* **2014**, *118*, 11007−11027.

(58) Marx, D.; Chandra, A.; Tuckerman, M. E. *Chem. Rev.* **2010**, *110*, 2174−2216.

(59) Vijay-Kumar, S.; Bugg, C. E.; Cook, W. J. *J. Mol. Biol.* **1987**, *194*, 531−544.

(60) Bushnell, G. W.; Louie, G. V.; Brayer, G. D. *J. Mol. Biol.* **1990**, *214*, 585−595.

(61) Maurus, R.; Overall, C. M.; Bogumil, R.; Luo, Y.; Mauk, A. G.; Smith, M.; Brayer, G. D. *Biochim. Biophys. Acta, Protein Struct. Mol. Enzymol.* **1997**, *1341*, 1−13.

(62) Ruotolo, B. T.; Benesch, J. L. P.; Sandercock, A. M.; Hyung, S.-J.; Robinson, C. V. *Nat. Protoc.* **2008**, *3*, 1139−1152.

(63) Mesleh, M. F.; Hunter, J. M.; Shvartsburg, A. A.; Schatz, G. C.; Jarrold, M. F. *J. Phys. Chem.* **1996**, *100*, 16082−16086.

(64) Abascal, J. L. F.; Vega, C. *J. Chem. Phys.* **2005**, *123*, 234505.

(65) Huang, J.; MacKerell, A. D. *J. Comput. Chem.* **2013**, *34*, 2135−2145.

(66) Li, L.; Vorobyov, I.; MacKerell, A. D.; Allen, T. W. *Biophys. J.* **2008**, *94*, L11−L13.

(67) Autenrieth, F.; Tajkhorshid, E.; Baudry, J.; Luthey-Schulten, Z. *J. Comput. Chem.* **2004**, *25*, 1613−1622.

(68) Piana, S.; Lindorff-Larsen, K.; Shaw, D. E. *Proc. Natl. Acad. Sci. U. S. A.* **2013**, *110*, 5915−5920.

(69) Verlet, L. *Phys. Rev.* **1967**, *159*, 98−103.

(70) Hess, B.; Henk, B.; Berendsen, H. J. C.; Fraaije, J. G. E. M. *J. Comput. Chem.* **1997**, *18*, 1463−1472.

(71) Miyamoto, S.; Kollman, P. A. *J. Comput. Chem.* **1992**, *13*, 952−962.

(72) Hoover, W. G. *Phys. Rev. A: At., Mol., Opt. Phys.* **1985**, *31*, 1695−1697.

(73) Wedekind, J.; Reguera, D.; Strey, R. *J. Chem. Phys.* **2007**, *127*, 0645011−06450112.

(74) Gabelica, V.; De Pauw, E. *Mass Spectrom. Rev.* **2005**, *24*, 566−587.

(75) Merenbloom, S. I.; Flick, T. G.; Williams, E. R. *J. Am. Soc. Mass Spectrom.* **2012**, *23*, 553−562.

(76) Mao, Y.; Woenckhaus, J.; Kolafa, J.; Ratner, M. A.; Jarrold, M. F. *J. Am. Chem. Soc.* **1999**, *121*, 2712−2721.

(77) Hopper, J. T. S.; Oldham, N. J. *J. Am. Soc. Mass Spectrom.* **2009**, *20*, 1851−1858.

(78) Grewal, R. N.; El Aribi, H.; Smith, J. C.; Rodriquez, C. F.; Hopkinson, A. C.; Siu, K. W. M. *Int. J. Mass Spectrom.* **2002**, *219*, 89−99.

(79) Van Berkel, G. J.; De La Mora, J. F.; Enke, C. G.; Cole, R. B.; Martinez-Sanchez, M.; Fenn, J. B. *J. Mass Spectrom.* **2000**, *35*, 939−952.

(80) Metwally, H.; McAllister, R. G.; Konermann, L. *Anal. Chem.* **2015**, *87*, 2434−2442.

(81) Fenn, J. B.; Rosell, J.; Meng, C. K. *J. Am. Soc. Mass Spectrom.* **1997**, *8*, 1147−1157.

(82) Kaltashov, I. A.; Mohimen, A. *Anal. Chem.* **2005**, *77*, 5370−5379.

(83) Kaminski, G.; Duffy, E. M.; Matsui, T.; Jorgensen, W. L. *J. Phys. Chem.* **1994**, *98*, 13077−13082.

(84) Cary, P. D.; King, D. S.; Crane-Robinson, C.; Bradbury, E. M.; Rabbani, A.; Goodwin, G. H.; Johns, E. W. *Eur. J. Biochem.* **1980**, *112*, 577−580.

(85) Vega, C.; de Miguel, E. *J. Chem. Phys.* **2007**, *126*, 154707.

(86) Shelimov, K. B.; Jarrold, M. F. *J. Am. Chem. Soc.* **1997**, *119*, 2987−2994.